LNF - 68/21
8 Aprile 1968

S. De Schryver, L. Fiore, S. Focardi, G. Gialanella, V. Rossi,
B. Stella and G. Susinno : TWO PION PHOTOPRODUCTION IN
A HYDROGEN BUBBLE CHAMBER BELOW 1000 MeV. -

LNF-68/21

S. De Schryver, L. Fiore[x], S. Focardi[o], G. Gialanella[x], V. Ros_
si[x], B. Stella, G. Susinno: "TWO PION PHOTOPRODUCTION IN A
HYDROGEN BUBBLE CHAMBER BELOW 1000 MeV".

1 - INTRODUCTION -

In this paper we report some preliminary results of an investiga_
tion on the double photoproduction reaction

(1) $\qquad \gamma + p \longrightarrow p + \pi^+ + \pi^-$

carried out by means of a hydrogen bubble chamber at the electron syn-
chrotron of the Laboratori Nazionali di Frascati.

In the past this reaction was analysed mainly with counter tech-
niques and only recently a collection of data with considerable statistics
was reached by hydrogen bubble chambers at the CEA and DESY labora-
tories[1,2].

(x) - Istituto di Fisica dell'Università di Roma and INFN, Sezione di
   Roma.
(o) - Istituto di Fisica dell'Università di Bologna and INFN, Sezione di
      Bologna.

This study of reaction (1) is a part of a systematic investigation of the photoproduction reactions with more than two bodies in the final state undertaken at Frascati with the bubble chamber technique in order to give a contribution to the knowledge of the photoproduction mechanism and of the formation of barionic and mesonic resonant states below 1000 MeV.

The main features of reaction (1), below 1000 MeV which seem to be experimentally well established, are as follows:

a) The shape of the total cross section, which goes up rapidly with the energy and has a maximum between 650 and 1000 MeV.

b) The formation of the Δ (N_{33}^x) isobar in the $\Delta^{++}(\pi^+ p)$ charge state, with a production percentage, which is nearly 100% from the threshold to 800 MeV and decreases to 70% at 1000 MeV.

c) Very low production, with a percentage consistent with zero, of the Δ isobar in the neutral charge state ($\pi^- p$).

The phenomenological models, which have been used so far to interpretate these features, are essentially of two kinds. In the first one the excitation of an intermediate isobar is assumed, according to the following scheme:

$$\gamma + p \longrightarrow N_{1/2}^x \longrightarrow \Delta + \pi$$
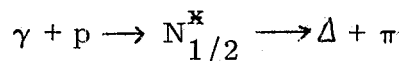
where $N_{1/2}^x$ is an isobar (πN) with T = 1/2 isospin[1]. The second one is the OPE model modified in order to achieve gauge invariance by adding to the OPE diagram, with suitable rules, the contribution of some other diagrams[3].

The predictions of both models agree satisfactorily well with the experimental results.

There are however some discrepancies as to the quantitative predictions which suggest the opportunity of further investigating this and other complementary processes in the energy range below 1000 MeV, and also attempting a different approach in the interpretation of the experimental data.

The present report consists of five sections. In section 2 we describe the experimental apparatus and the modifications introduced in the bubble chamber in order to expose it to the photon beam; in section 3 we report the criteria adopted in the analysis of the events. The experimental results are shown and discussed in section 4 and 5 respectively.

2 - EXPERIMENTAL APPARATUS -

The bubble chamber used was constructed at the CERN laboratories and operated there until 1962. In 1965 it was carried to the Laboratori Nazionali di Frascati.

The chamber has a cylindrical body with a 32 cm diameter and a 15 cm depth and is placed in a 17 KGauss magnetic field.

In fig. 1 a picture of the bubble chamber is shown. The main modification introduced for this experiment is the beam entrance window. It consists of a 0.25 mm thick mylar foil (6 x 1.5 cm^2), in order to minimize the electromagnetic background. In such a way, the beam, before entering the chamber, passes through about 10^{-3} radiation lengths, which correspond to 1/30 of the hydrogen thickness in the chamber.

For safety reasons the window is enclosed in a 3.5 m long stainless steel tube, which, in the case of breaking of the mylar window, prevents hydrogen escape. In Fig. 2 some details of this part are shown.

The electromagnetic background produced in the 0.5 mm thick tube plug is removed by a clearing magnetic field and by a collimator placed in the tube itself.

In Fig. 3 the overall experimental set up is shown. The bremsstrahlung beam was produced by spilling the circulating electrons in the synchrotron onto a 0.1 radiation length thick tantalium target. The compatibility with other simultaneous beam users was achieved by setting up the target every time with a suitable current pulse synchronized with the bubble chamber expansion.

The photon beam is hardened by means of 6 radiation lengths of LiH, which also reduce its intensity to suitable values, while mantaining the maximum circulating beam current in the synchrotron.

We will discuss in the next section the measurement of the γ-ray spectrum. However we anticipate here that the hardener thickness, chosen in order to obtain the best photon beam intensity, was probably too high; in fact, we observed a regeneration of photons with intermediate energies, due to the process of secondary bremsstrahlung taking place in the absorber itself.

The bubble chamber analyzing magnet was feeded by a Graetz bridge rectifier realized with silicon diodes.

In Fig. 4 the scheme of the rectifier is shown. Each diode (Philips BYX1600) carries a current of 150 A. The output of rectifier current is 2000 A at 500 V. The alternate component is filtered by the inductance of the magnet coils so that the ripple factor becomes less than 1%.

To overcome the lack of current stabilization, we have introduced in the magnet a field meter whose output, in digital form, is photographed in every picture.

In the Appendix some details are given of the auxiliary electronic equipment together with a brief description of the external monitoring system used to measure the photon flux.
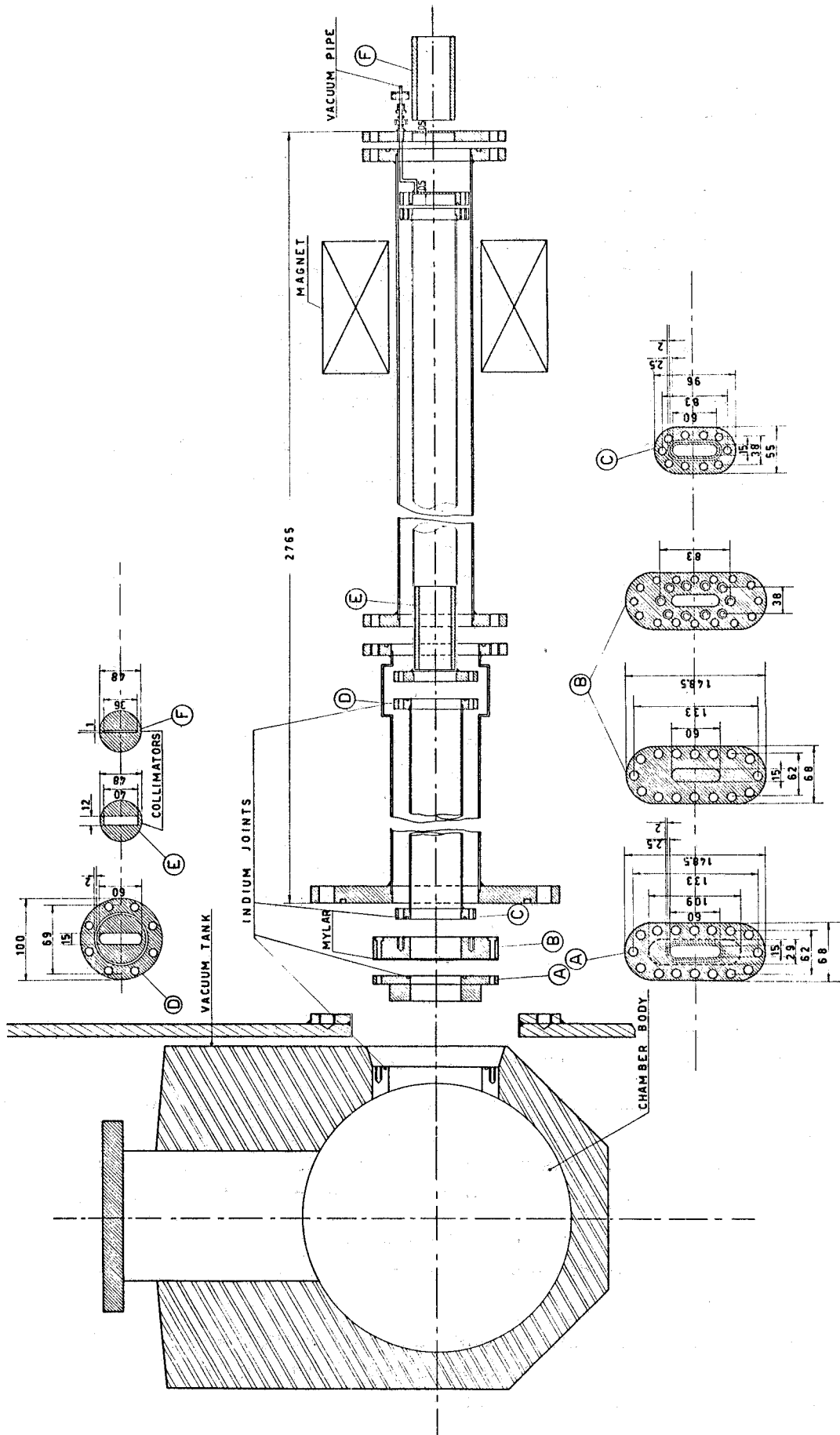
4.

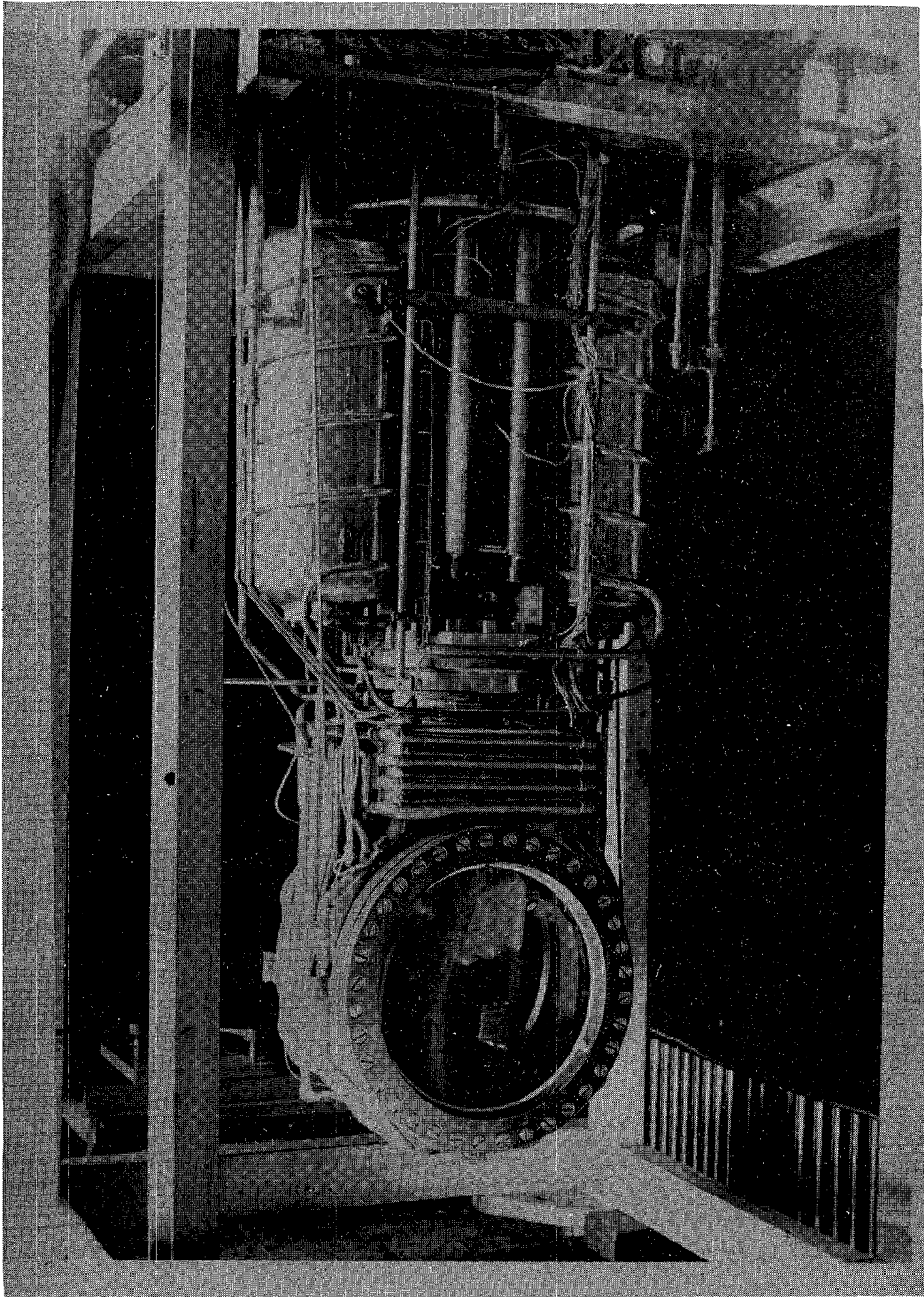FIG. 2 – Assembling of the beam entrance.
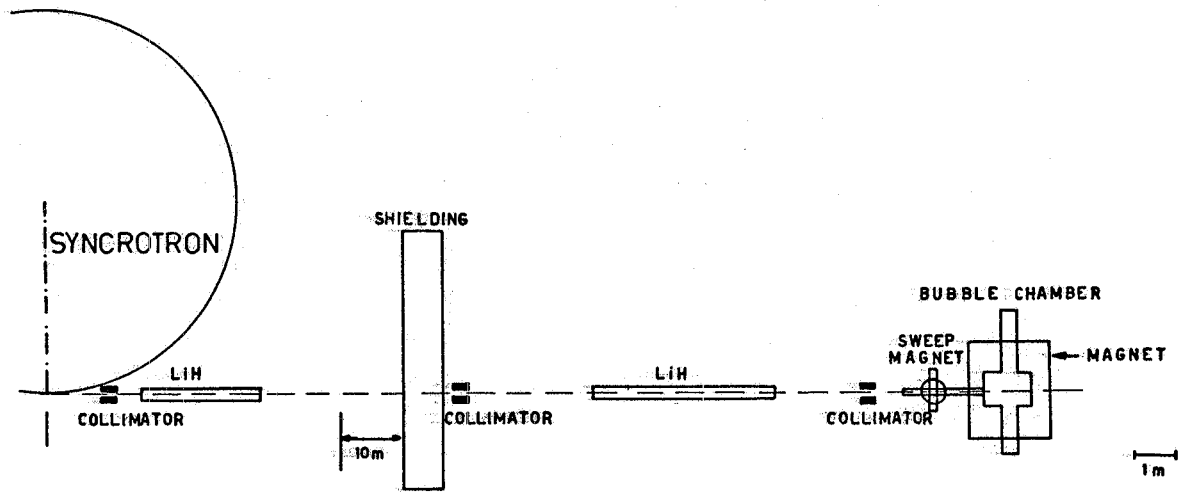
FIG. 1 - The 32 HBC CERN bubble chamber.
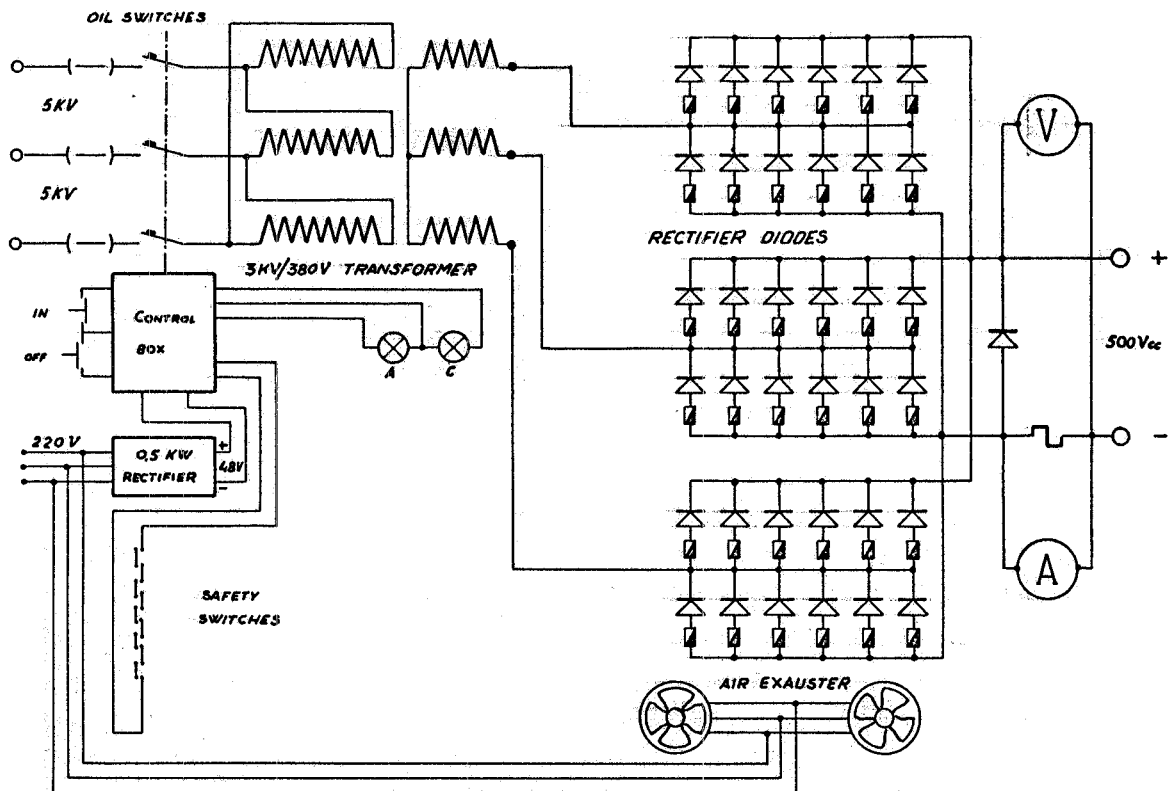
FIG. 3 - Experimental set-up.

FIG. 4 - Schema of the rectifier used to feed the magnet of the bubble chamber.

3 - CHAMBER EXPOSURE AND ANALYSIS OF THE EVENTS -

About 400.000 pictures were taken at different photon beam inten sities. In this report we present the results of the analysis of the first 200.000 pictures, which were taken with a beam intensity of about 300 e-quivalent quanta per pulse, corresponding to about 10 e^+e^- pairs per picture. In fig. 5 a typical photo with a double photoproduction event is shown. Successively the photon beam intensity was increased by a factor about 2. This increase becomes possible by setting an external monitoring system, which furnished the incident photon flux, without necessity of counting the e^+e^- pairs produced in the chamber. In such a way the frequency of the three-prong events rised from 1 per 100 pictures to 1 per 50 pictures, without reducing the measurability nor the scanning efficiency.

Part of the film was scanned twice so obtaining an overall efficiency about 99% (90% for each scanning). The events are easily distinguishable from the electromagnetic background also with 25-30 e^+e^- pairs per picture. In fact the events under study have three prongs, one of which (the proton) is almost always very ionizing.

The measurements were carried out with "mangiaspago" digitized apparatus, which have a precision of 0.1 mm on the projection table.

The geometrical reconstruction of the events and the kinematical calculations were accomplished with the standard THRESH and GRIND programs on IBM 7040 and 7094 computers.

Since the angles and momenta of the three charged particles in the final state were measured, the direction of the incoming photon (but not its energy) and the masses of all particles were known, the kinematics of reaction (1) was over determined and a 3C-fit was possible. This allowed us to distinguish the triple photoproduction events

(2) $$\gamma + p \longrightarrow p + \pi^+ + \pi^- + \pi^0$$

(3) $$\gamma + p \longrightarrow n + \pi^+ + \pi^+ + \pi^-$$
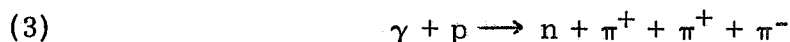
making also the kinematical reconstruction more accurate.

The mean error in the measurement of the charged particle momen ta after the fit is $\pm$ 5%. The error on the angle measurements is $\pm$ 0.1°. The photon energy is determined with a mean error of $\pm$ 4%. The mean er ror (due to the above ones) in the determination of the squared mass of the $p\pi^+$, $p\pi^-$ and $\pi^+\pi^-$ systems are $\pm$ 270 MeV^2, $\pm$ 300 MeV^2 and $\pm$ 100 MeV^2 respectively.

If we assign the mass of the neutral particle, also the kinematics of the events (2) and (3) is determined, but a fit is not possible (OC).

In Fig. 6 the experimental distribution of the χ^2 resulting from the 3C fits is shown. An event is accepted only if $\chi^2 \leq 10 (P(\chi^2) \geq 0.02)$.
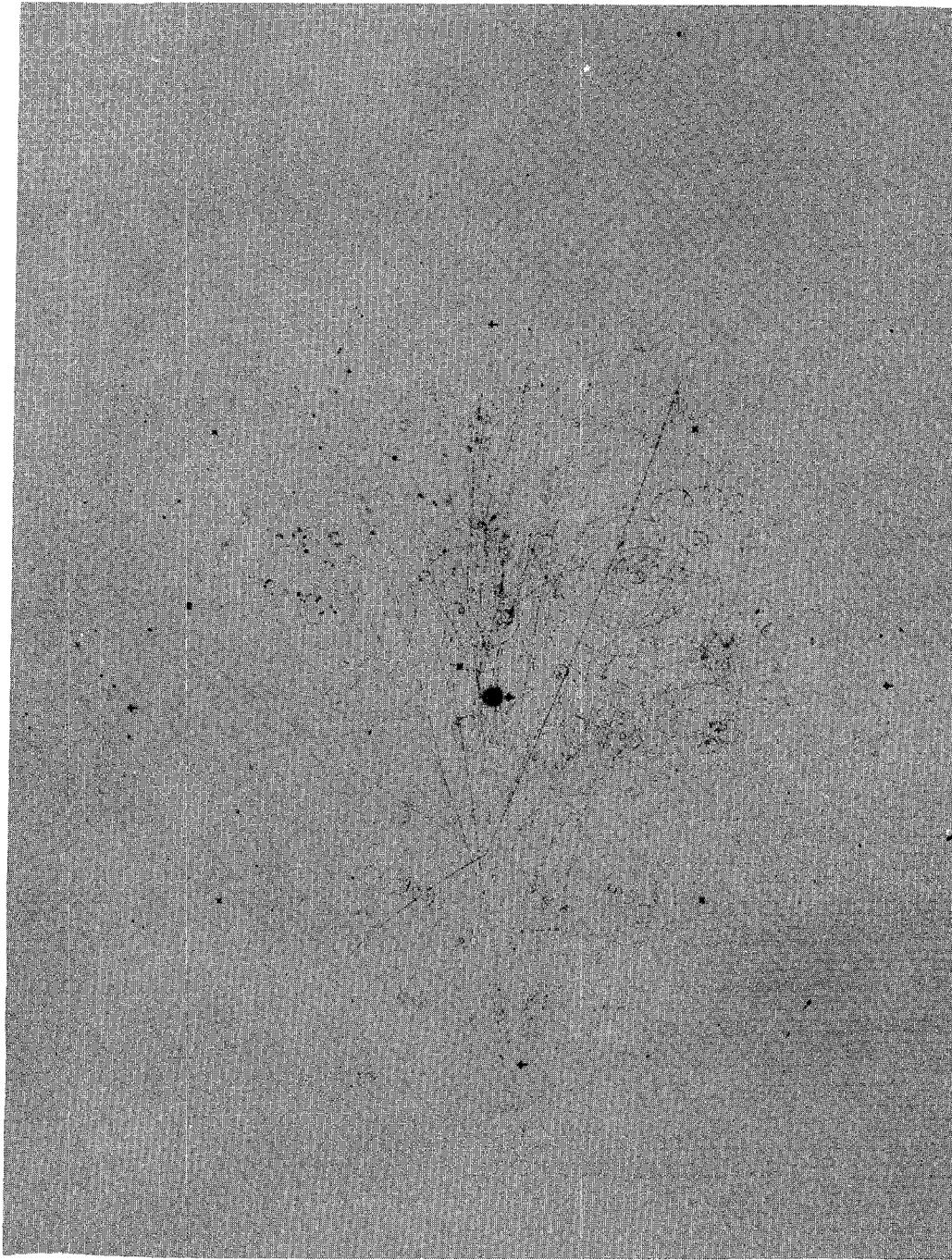
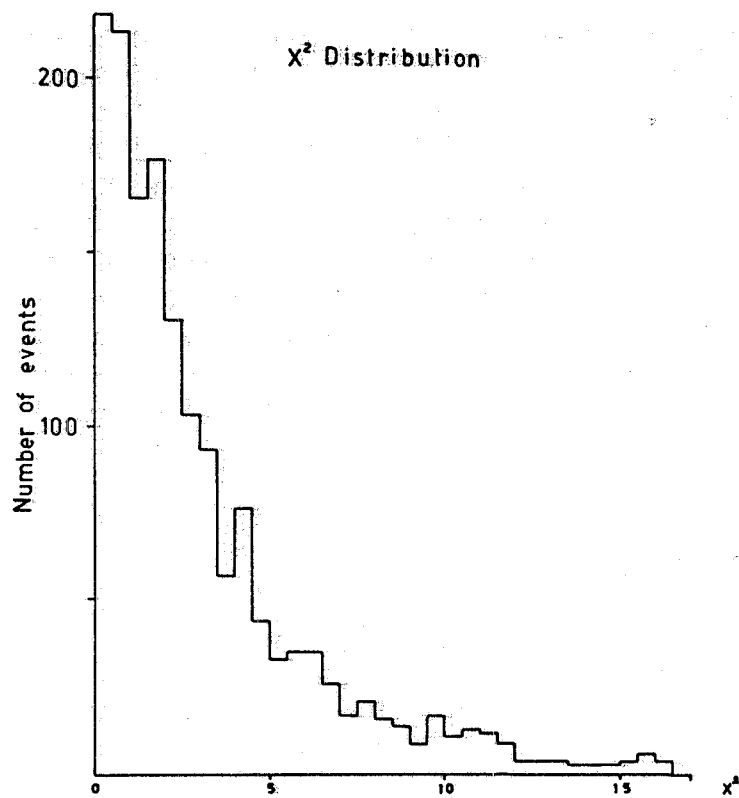FIG. 5 - A typical picture with a double photoproduction event.

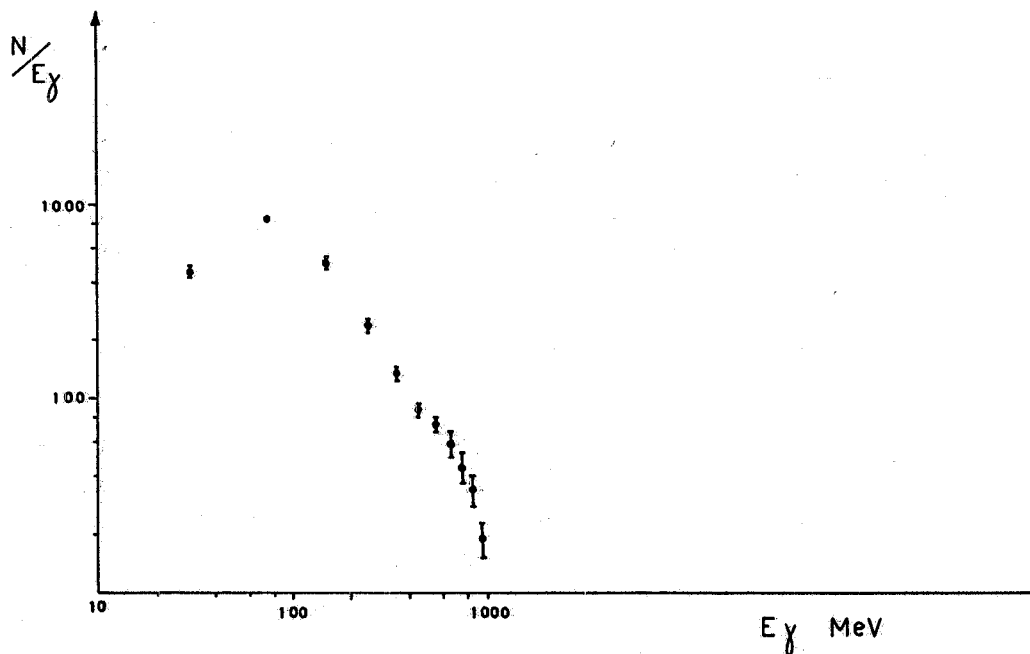FIG. 6 - Experimental distribution of the χ^2 for the 3C fit events.

FIG. 7 - Measured energy spectrum of the photons entering the bubble chamber. The measurement was carried out on about 4000 e^+ e^- pairs distributed in the whole film.

The direction of the incoming photon was obtained by the measurements of the e^+e^- pairs. The γ-ray spectrum was obtained by measuring the momenta and angles of the e^+e^- pairs and is shown in Fig. 7. For this measurement it was necessary to eliminate the pictures with too many tracks in order to avoid a choice of the measurable pairs. We decided to measure the electrons only in the pictures in which all pairs were measurable. Besides, the fiducial volume was reduced for the pairs respect to that for the events. The experimental data of Fig. 7 were obtained from the measurements of about 4000 pairs distributed in the whole film. The maximum photon energy was 1000 MeV. As we can see the LiH absorber hardens the beam for photon energies below 100 MeV and it also reduces the beam intensity in the high energy region.

4 - EXPERIMENTAL RESULTS -

Table I shows, for reaction (1), the number of the events found in a fiducial volume having the same section of the photon beam and extending 24 cm along its direction. This ensures the tracks to have a sufficient length to permit a good measurement in any case.

TABLE I

Photon energy (MeV)	Number of events
350-550	233
550-650	426
650-800	465
800-1000	368

In Fig. 8 the distributions of the angles φ and λ of the incident photons are shown, φ being the angle in the picture plane and λ the dip angle. From these graphs the beam direction results in being known with a standard deviation of $\pm 0.05^\circ$. Fig. 9 shows the behaviour of the total cross section of reaction (1) versus the incident γ-ray energy.

For comparison the results of other bubble chamber experiments[1, 2] are also reported.

Since the evaluation of the incident photon flux is at present not yet accomplished, our data are normalized to the above ones. The stated errors take into account the statistical uncertainty on the number of the events and on the measured photon spectrum.

Fig. 10 shows the distributions in the laboratory system of the angle α between the production plane of each particle and a reference plane. The isotropy of this angle ensures that there is no detection bias.

In Figs. 11 to 22 the experimental distributions of some kinematical quantities in the laboratory system are reported.
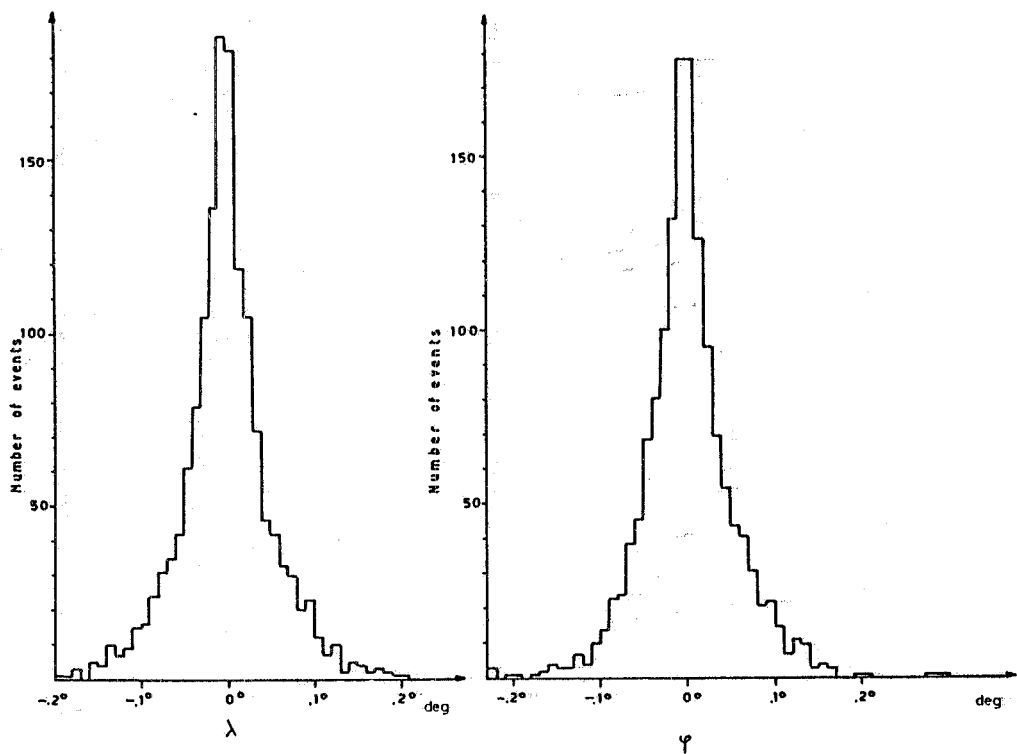
FIG. 8 - Angular distribution of the incident photons as a function of the projected angle φ in the film plane and as a function of the dip angle λ .
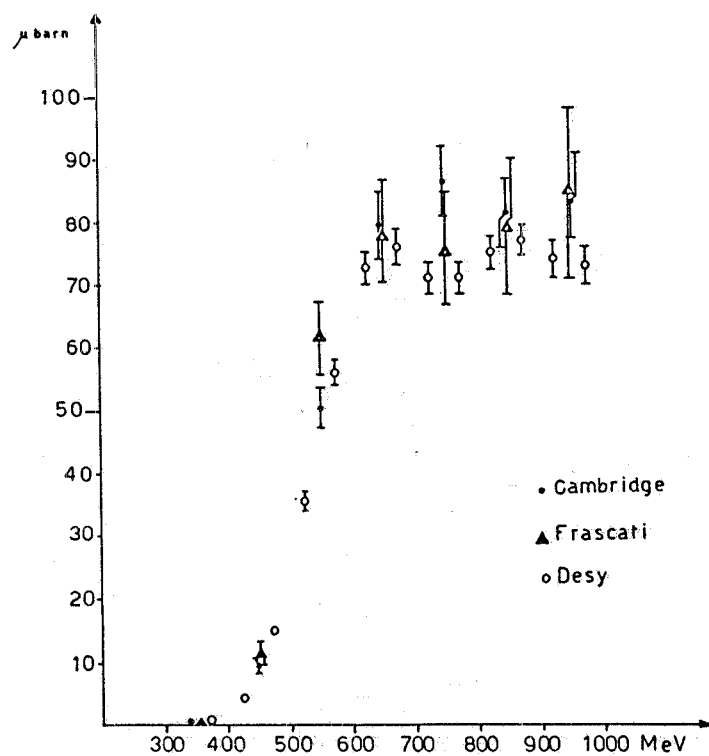

FIG. 9 - Total cross section for the reaction $\gamma + p \rightarrow p + \pi^+ + \pi^-$. For comparison the data of previous bubble chamber experiments are reported.
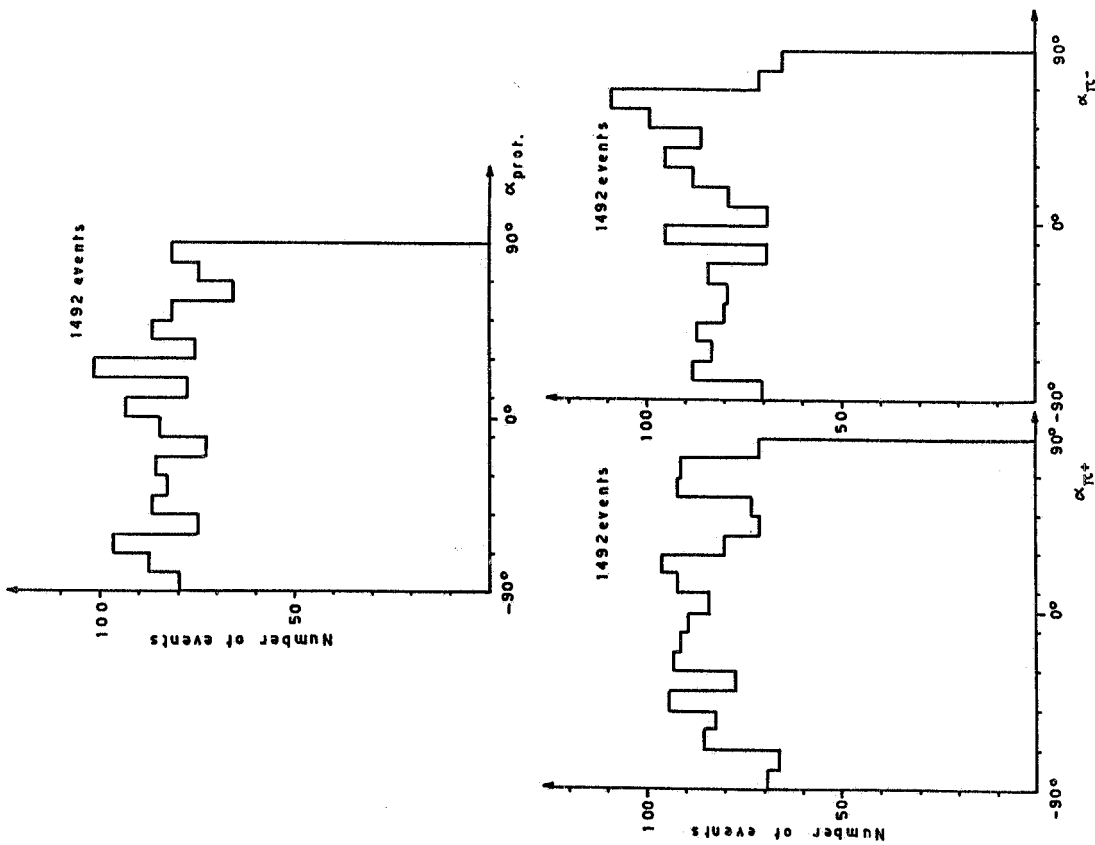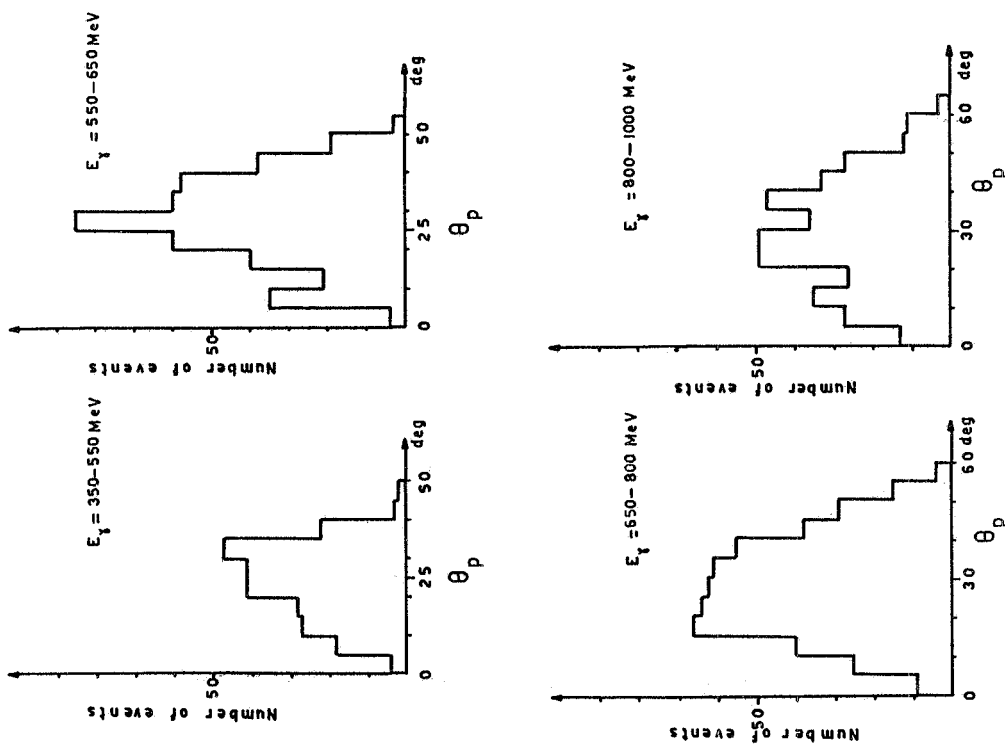
10.

FIG. 11 - Distribution of the angle θ_p between the proton and the photon directions for different photons energies.
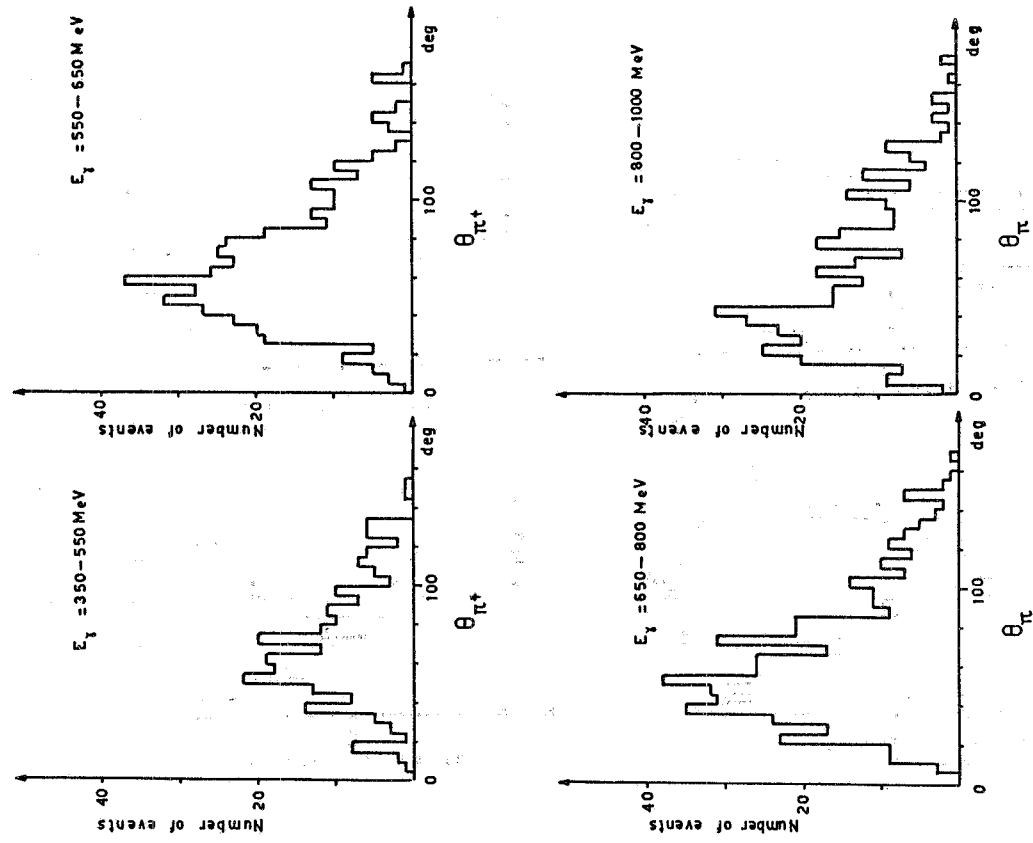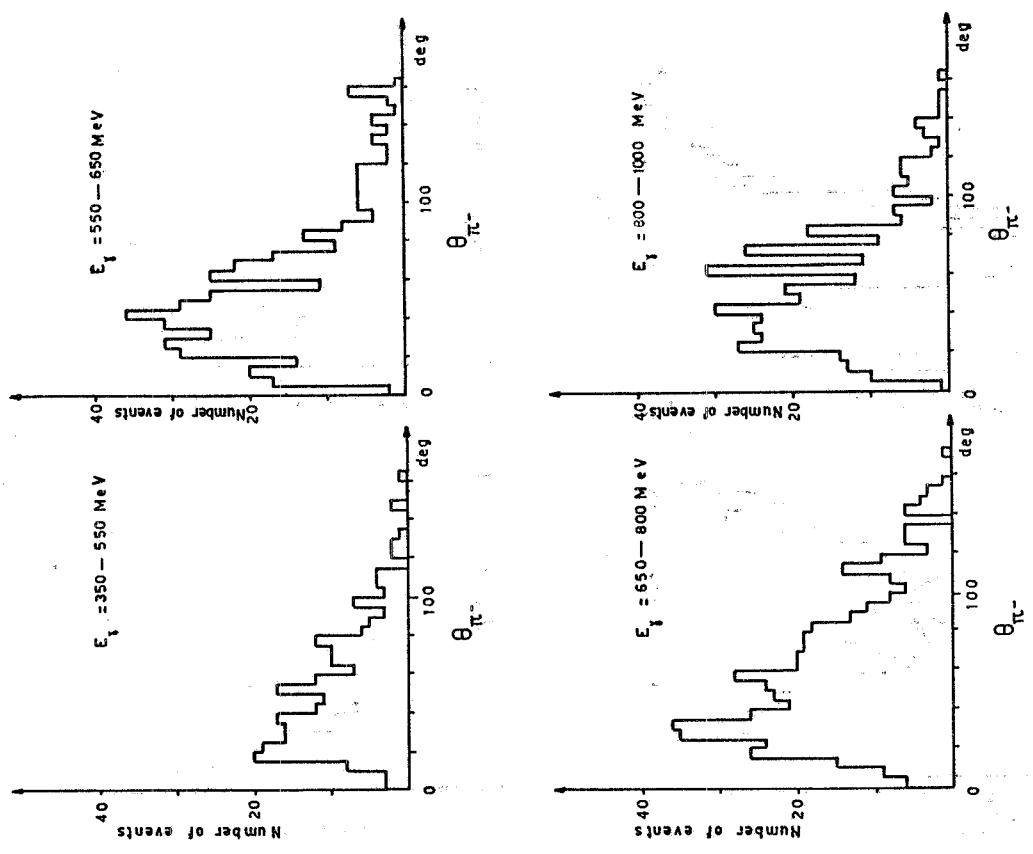

FIG. 10 - Distribution of the laboratory angle α between the production plane of each particle and the film plane.

FIG. 13 – Distribution of the angle θ_{π^-} between the π^- and the photon directions for different photons energies.
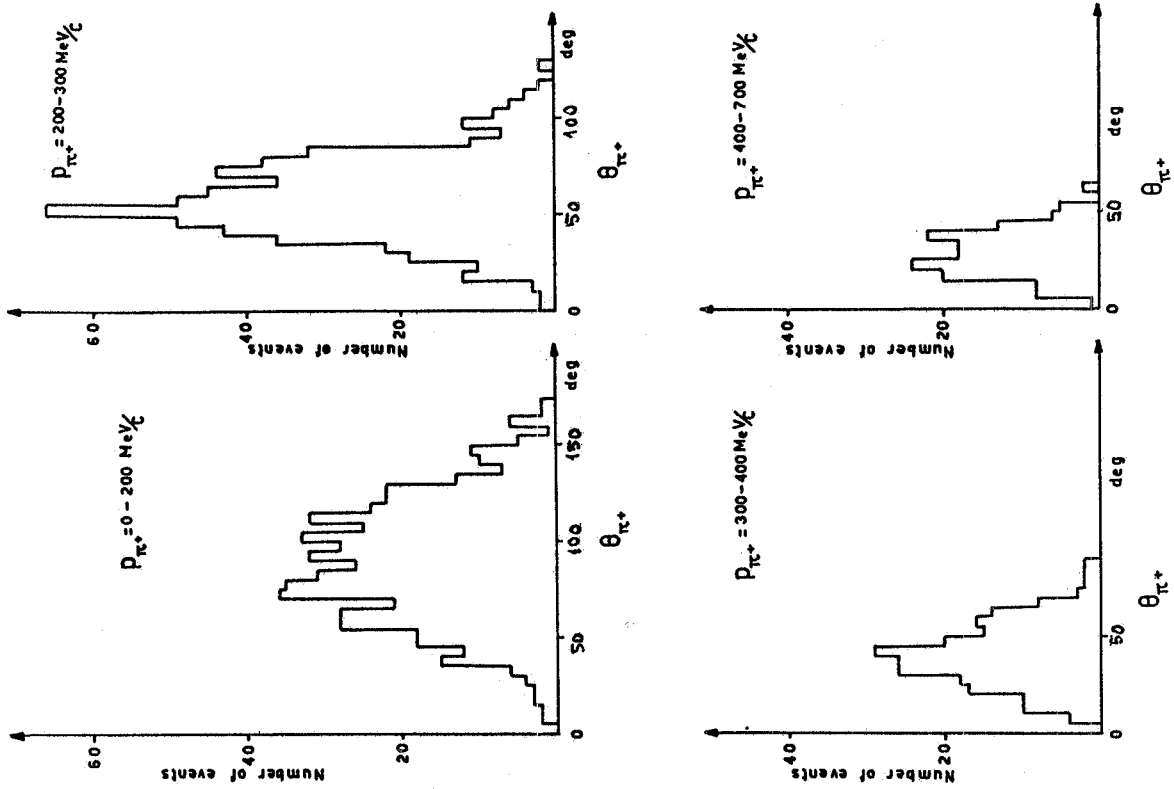

FIG. 12 – Distribution of the angle θ_{π^+} between the π^+ and the photon directions for different photons energies.

FIG. 15 – Distribution of θ_{π^+} angle for different va-
lues of the π^+ momentum.
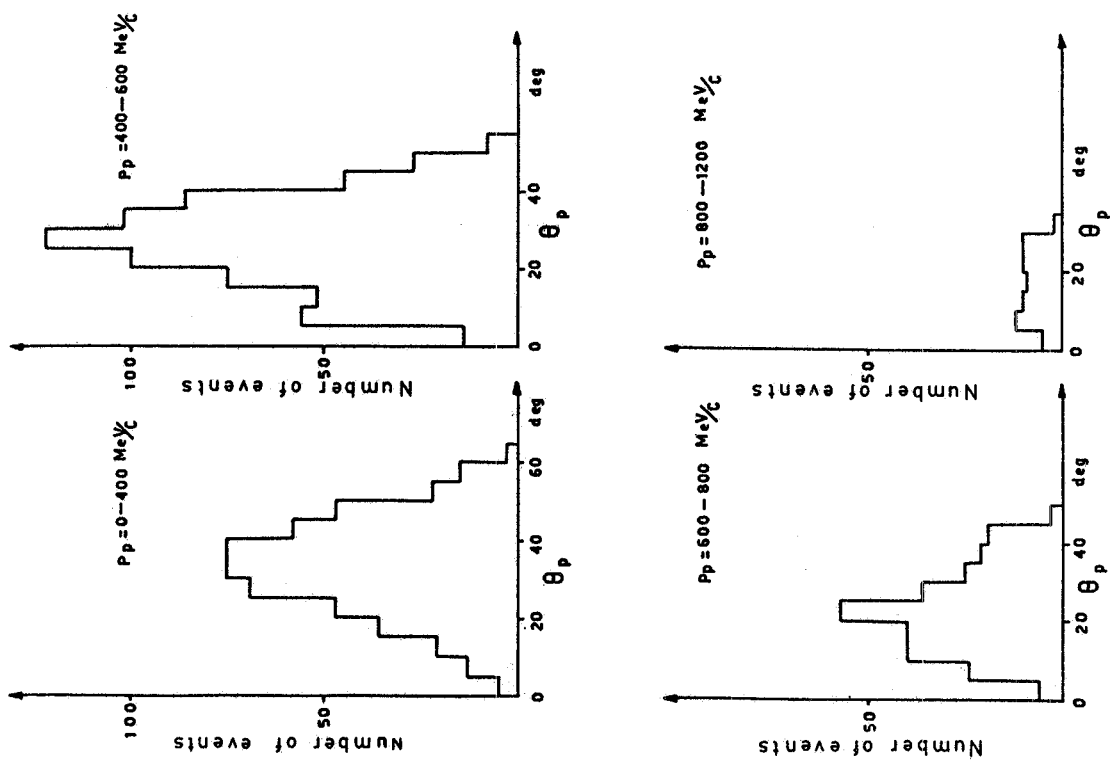
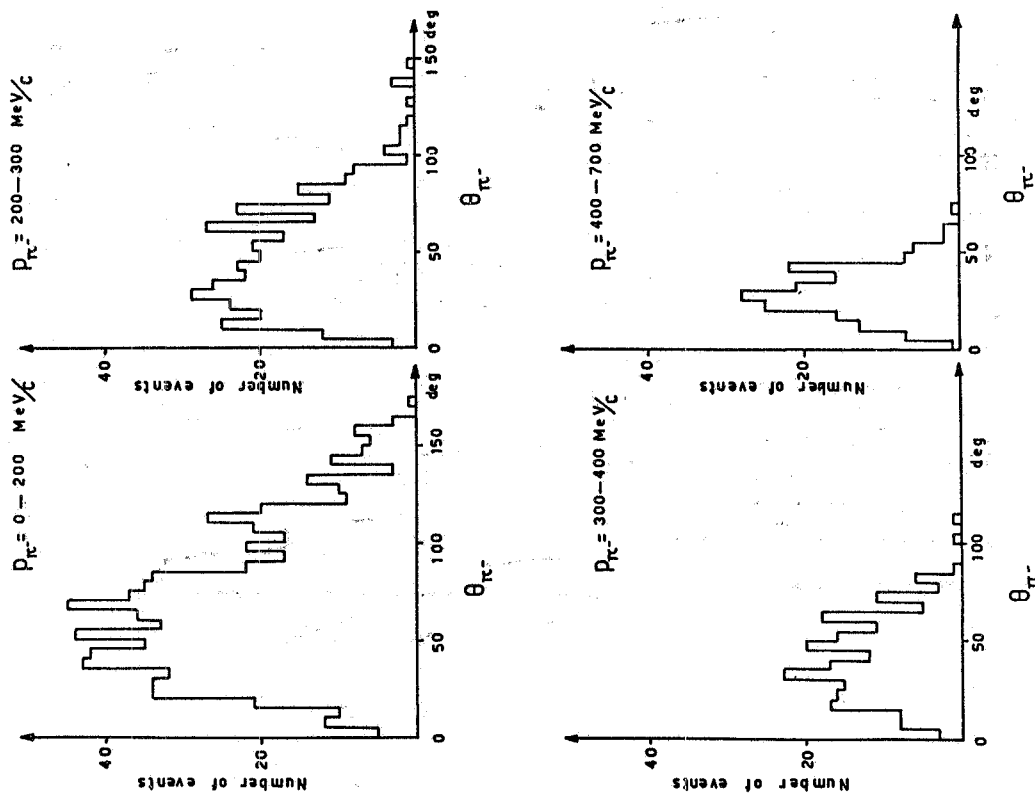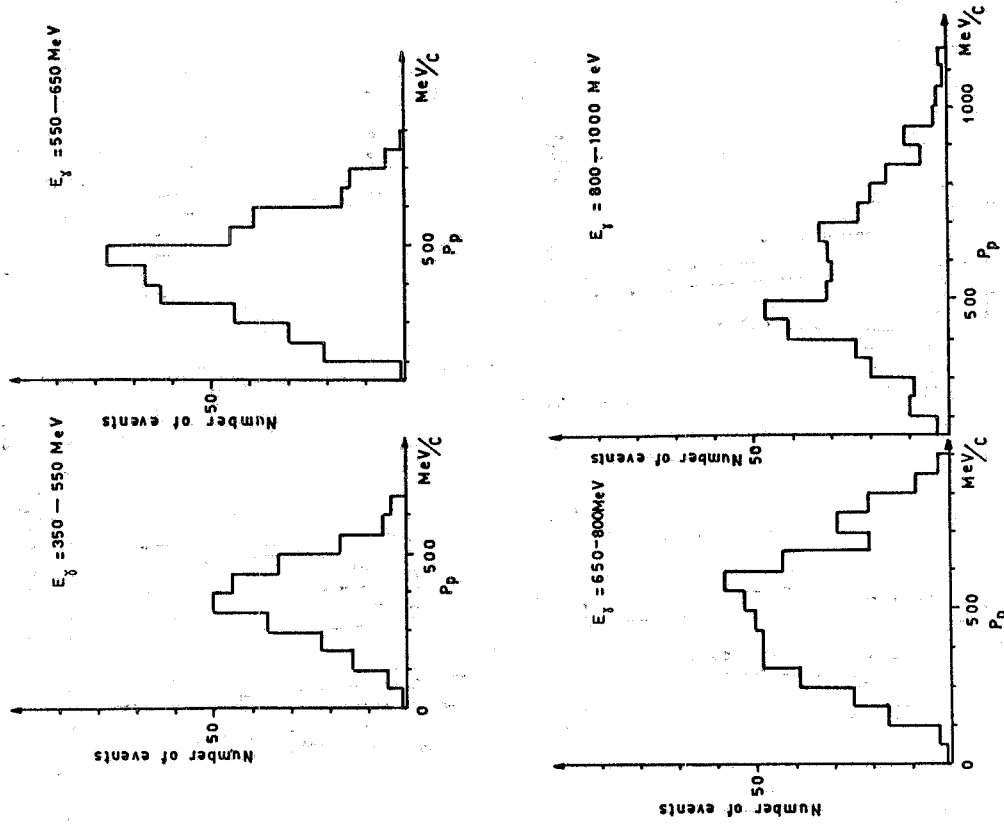FIG. 14 – Distribution of θ_p angle for different
values of the proton momentum

FIG. 17 – Distribution of the proton momentum for different photon energies.

FIG. 16 – Distribution of θ_{π^-} angle for different va lues of the π^- momentum.
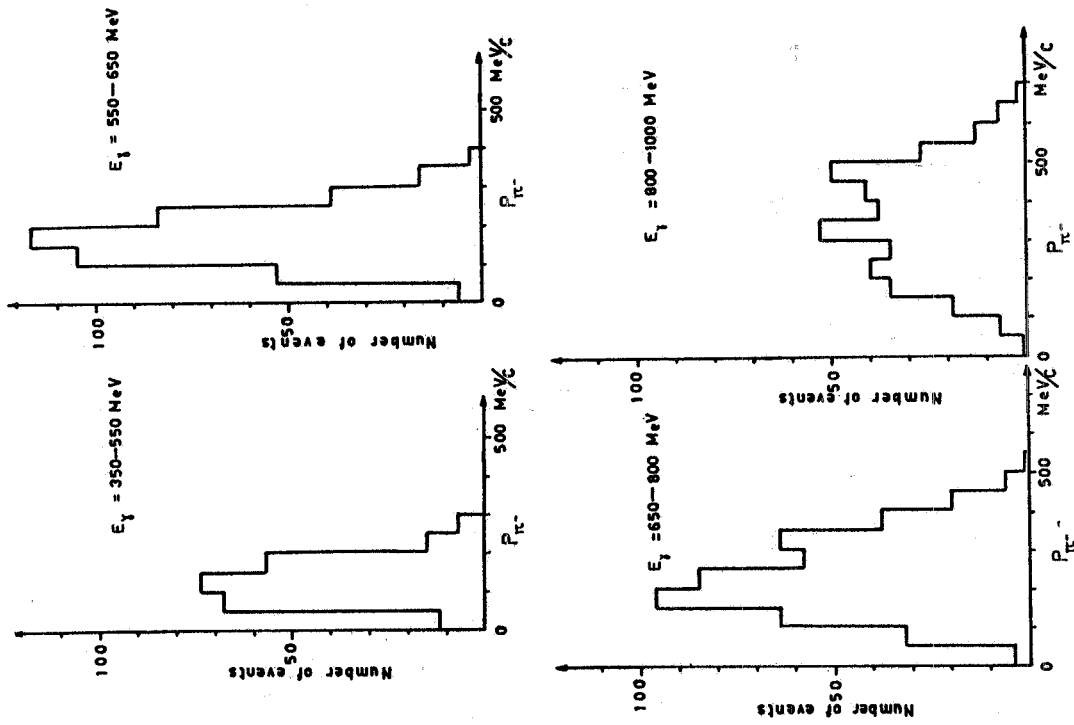
14.

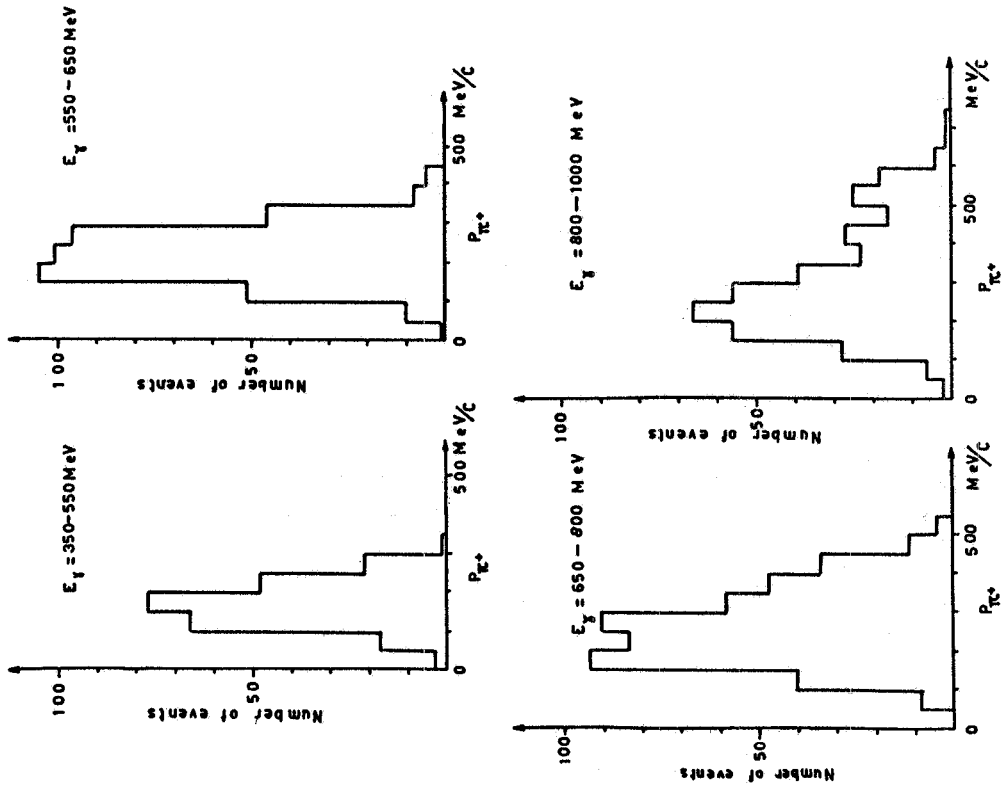FIG. 19 – Distribution of the π^- momentum for different photon energies.

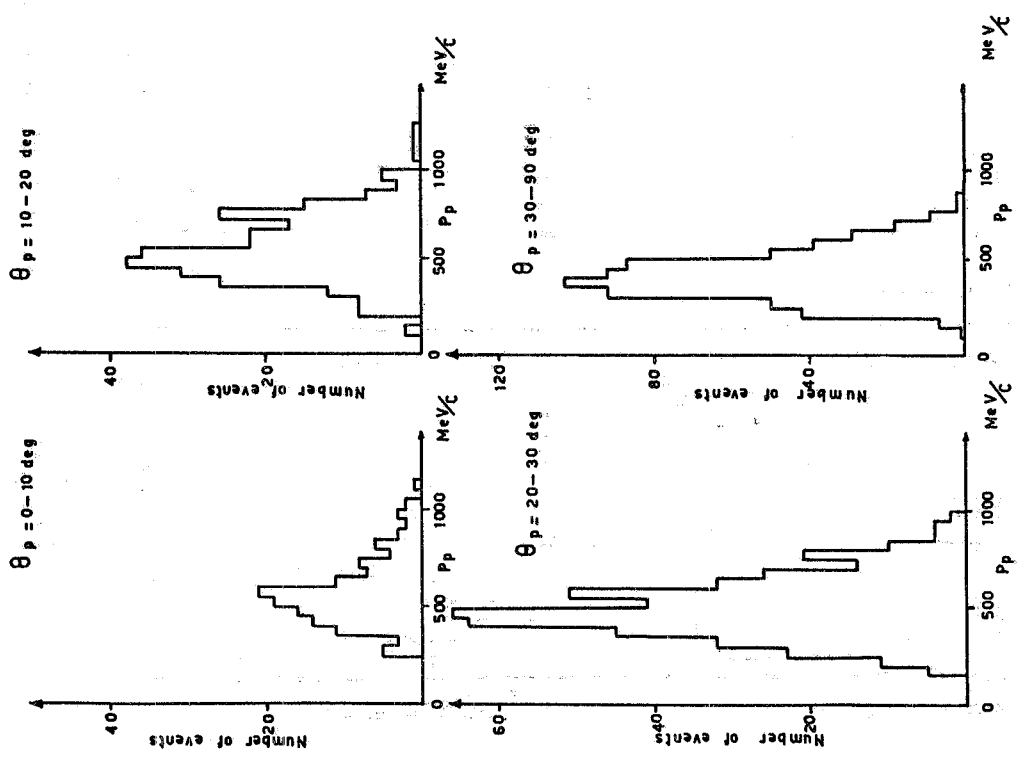FIG. 18 – Distribution of the π^+ momentum for different photon energies.

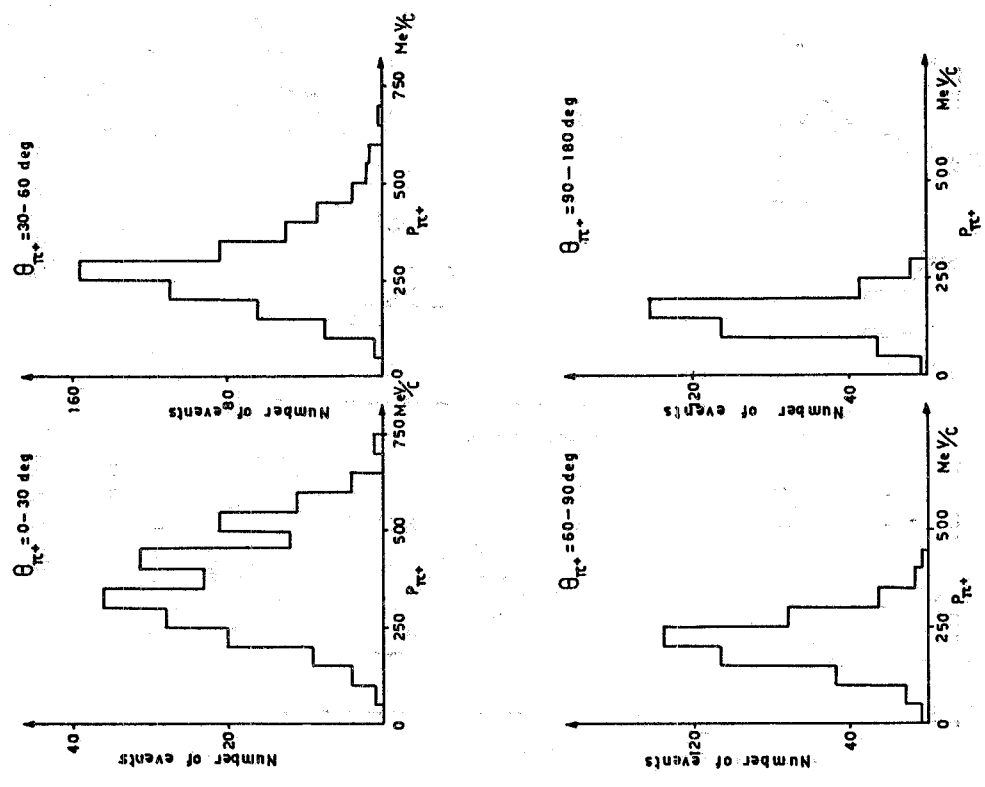FIG. 21 – Distribution of the π^+ momentum for different θ_{π^+} values.

FIG. 20 – Distribution of the proton momentum for different θ_p values.
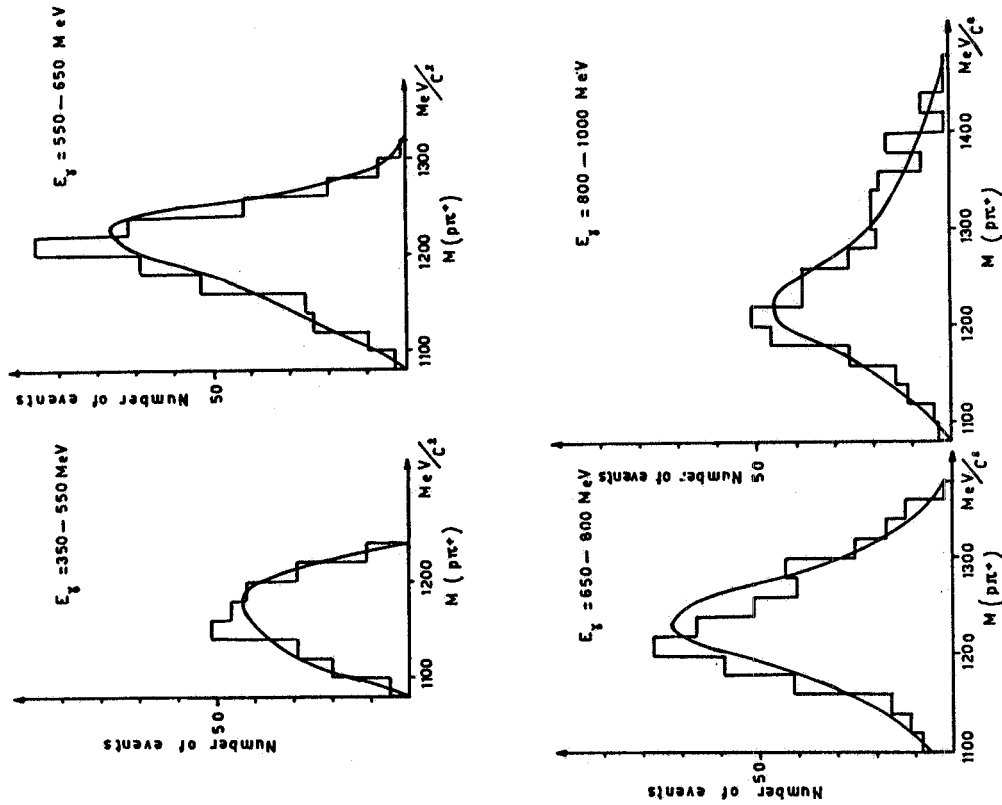
FIG. 23 - Distributions of the ($p\pi^+$) equivalent mass for different photon energies. The curves represent the calculated distributions for the mixture of the phase-space and of a Breit-Wigner resonance for the Δ_{33}-isobar, that better fits the experimental data.
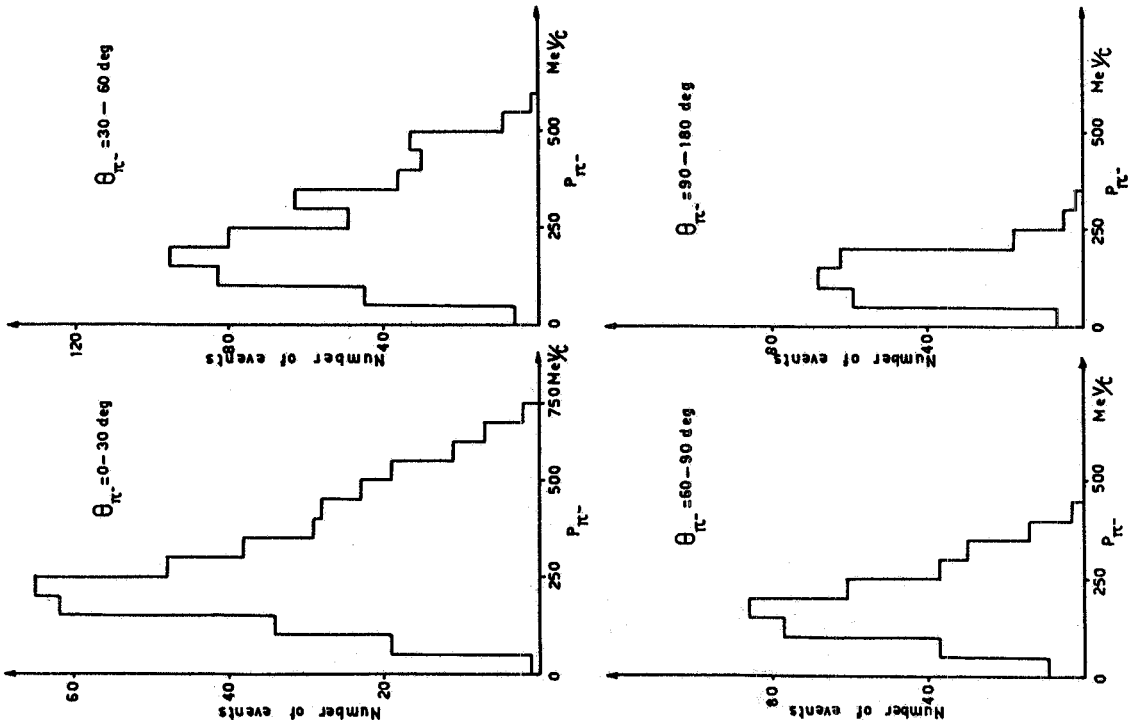

FIG. 22 - Distribution of the π^- momentum for different θ_{π^-} values.

5 - DISCUSSION OF THE RESULTS -

The main feature of reaction (1) below 1000 MeV is the very abundant formation of the Δ (1236) isobar in the doubly charged state ($\pi^+ p$), due to the P_{33} wave in the (πN) interaction. In Fig. 23 the distribution of the equivalent mass of the ($p\pi^+$) system is shown for different photon energies. The continuous curve is calculated by fitting to the experimental data a suitable incoherent mixture of the phase-space and a Breit-Wigner resonance for the Δ isobar. We have made two fits. In the first one the mixture percentages and the mass and width of the resonance were free. In the second one the resonance parameters (M = 1236 MeV, Γ = 120 MeV) were fixed and the only percentages had to be fitted. The results of the fits for different photon energies are reported in Table II.

By using the Monte Carlo method (OWL program) we have computed the reflection of the Δ^{++} isobar on the mass distribution of the ($p\pi^-$) and ($\pi^+\pi^-$) systems.

TABLE II

E_γ (MeV)	I Fit				II Fit	
	% Δ	$\dfrac{M(\Delta)}{MeV}$	Γ MeV	$P(X^2)$	% Δ	$P(X^2)$
350 - 550	100 ± 10	1208	102	0.10	100 ± 10	0.15
550 - 650	90 ± 10	1216	86	0.50	85 ± 10	< 0.01
650 - 800	100 ± 10	1231	132	< 0.01	90 ± 10	< 0.01
800 - 1000	65 ± 6	1232	94	0.25	70 ± 10	0.35

Our experimental mass distributions were compared with a suitable mixture of this reflection and phase space in the previously calculated percentages (Figs. 24 and 25). The comparison confirms the abundant formation of the Δ^{++} isobar, while there is no statistically significant evidence of the neutral $\Delta^0(\pi^- p)$ state in accordance with other previous experimental results[2]. On the other hand the ratio R = $\sigma(\Delta^0)/\sigma(\Delta^{++})$ expected by the OPE model as well by assuming that reaction (1) goes through an intermediate T = 1/2 state, is 1/9, still consistent with our present results.

As to the ($\pi^+\pi^-$) system, our present data are unsufficient to draw any conclusion about the presence of a resonant state (the so called σ-meson, M $\approx$ 400 MeV, T = J = 0), some evidence of which was found in a previous photoproduction experiments[4].
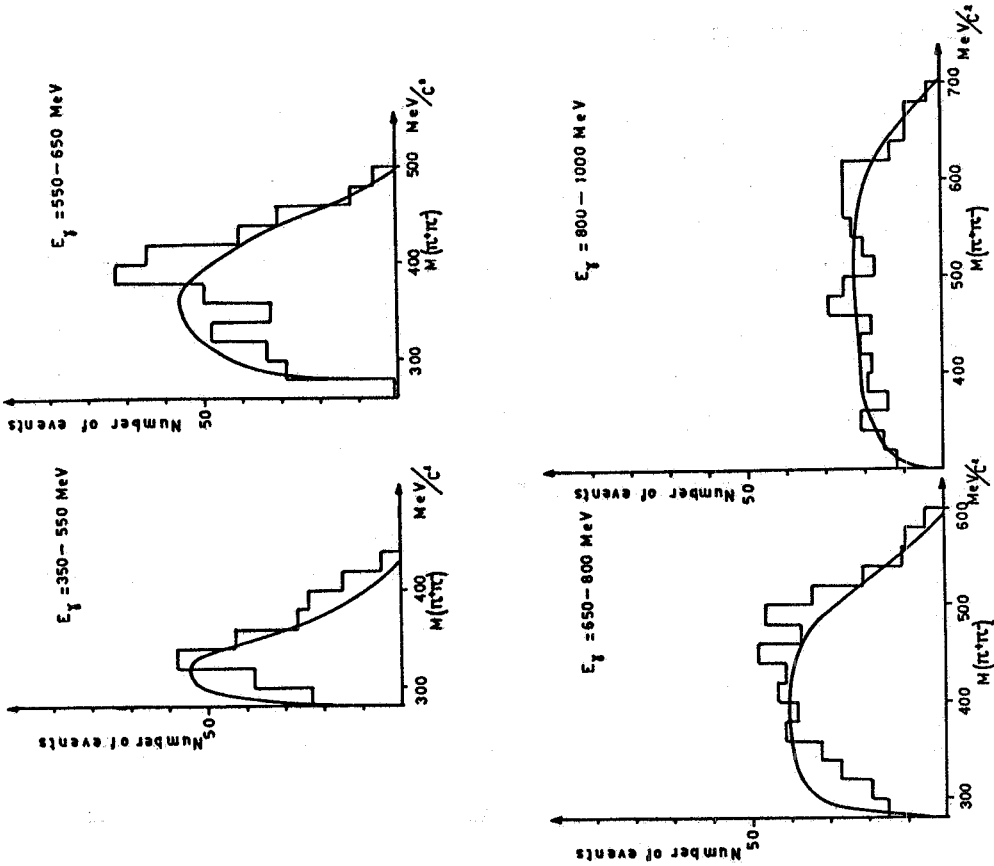
18.

FIG. 25 – Distribution of the $(\pi^+\pi^-)$ equivalent mass for different photon energies. The curves represent the calculated distributions, taking into account the reflection of the Δ^{++}.
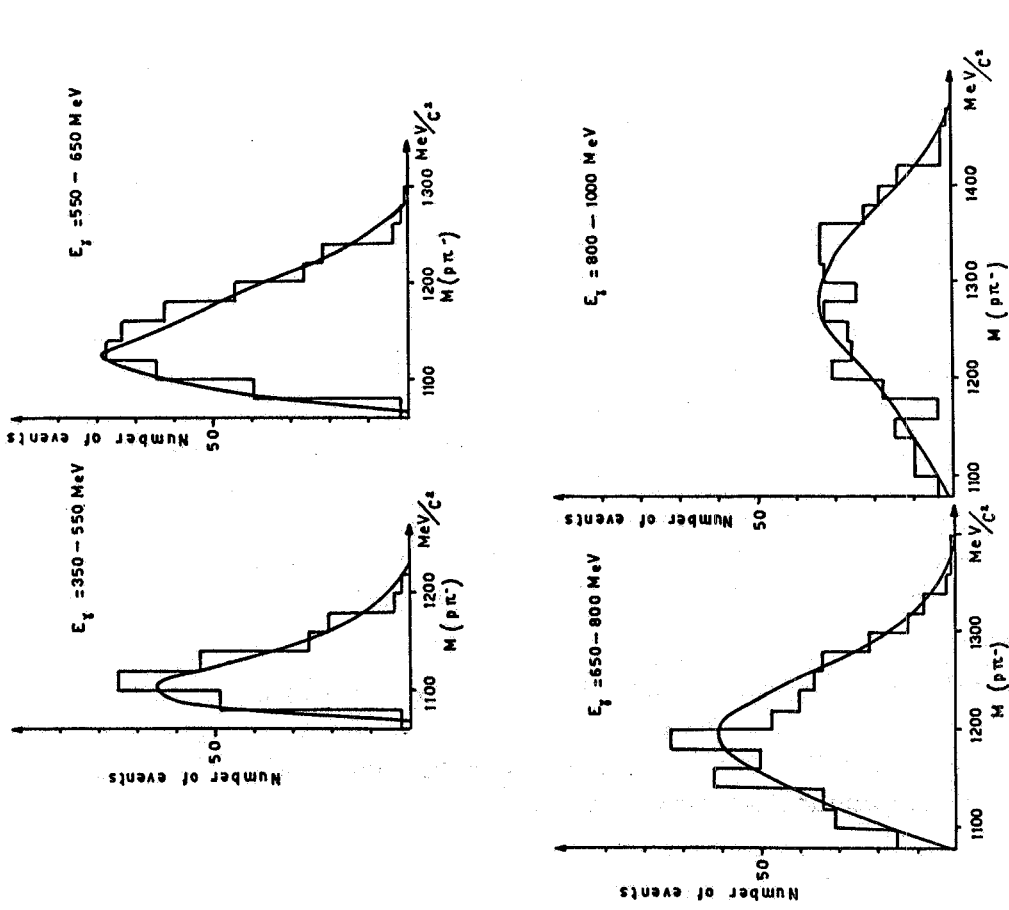
FIG. 24 – Distributions of the $(p\pi^-)$ equivalent mass for different photon energies. The curves represent the calculated distributions, taking into account the reflection of the $\overline{\Delta^{++}}$.

The interpretation of our experimental results is still in progress.

ACKNOWLEDGEMENTS -

APPENDIX - ELECTRONIC EQUIPMENT OF THE BUBBLE CHAMBER -

In this appendix a brief description of the circuitry which operates and controls the bubble chamber is given. The whole equipment can be subdivided in two groups:

- control of the chamber expansion and of the photographic apparatus;
- measurement of the magnetic field and monitoring of the incident photon flux.

All the circuits are controlled by a T_0 - pulse generator which ensures the timing of all the operations with the beam arrival and also allows the choice of the most suitable expansion rate.

A - CONTROL OF THE CHAMBER EXPANSION AND OF THE PHOTO-GRAPHIC APPARATUS -

In Fig. A.1 the general diagram is shown. The T_0-pulse generator controlled the chamber expansion, the target positioning and the length of the beam spill-out. The flash lighting was operated by an interlock system triggered by the integrated pulse of a scintillation counter placed on the photon beam after the chamber. In such a way it was possible to take pictures only when the photon intensity was included in an a priori selected range. Furthermore the flash light controlled, through a photodiode, the picture numeration and the film movement. The piston stroke, which causes the chamber expansion, as well as the instantaneous values at the pressure in the chamber and the level of the liquid hydrogen in the reservoir were minitored by suitable devices consisting essentially in a variable capacitor.

The variation of this capacity is measured by comparison with a known capacitance by means of the circuit shown in Fig. A2. A radiofrequency signal is applied to the circuit and the output signal, after demodulation, is sent to an oscilloscope. The changes of capacity to be measured are of the 3% at most and the actual values are of the order of 100 pF or less. Particular care was taken in order to reduce the cable capacitances.

In Fig. A.3 a typical oscilloscope picture is shown. The upper track measures the piston stroke and the lower one the pressure value in the chamber. The horizontal scale is 20 ms/cm and the vertical one 0.5 V/cm. On the lower track the beam pulse is also visible.

B - MAGNETIC FIELD MEASUREMENT AND MONITORING OF THE INCIDENT PHOTON FLUX -

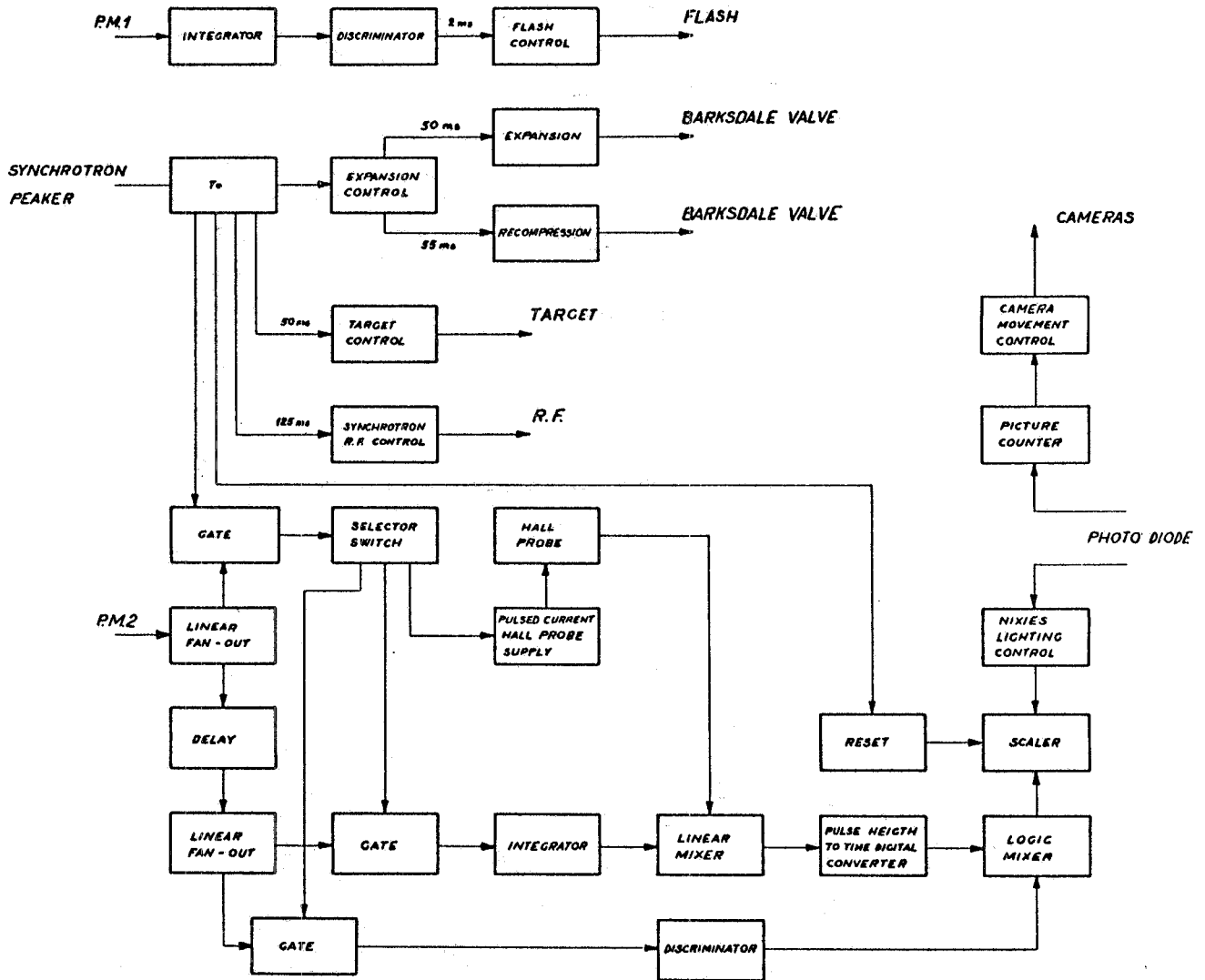As previously mentioned, it was necessary to measure the magne-

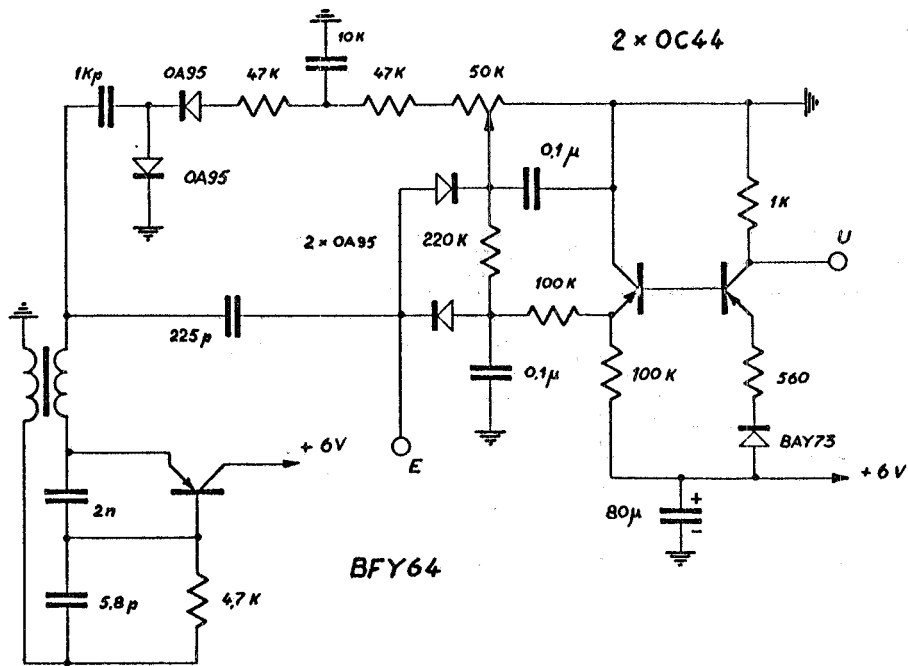FIG. A. 1 - General block diagram of the electronics.

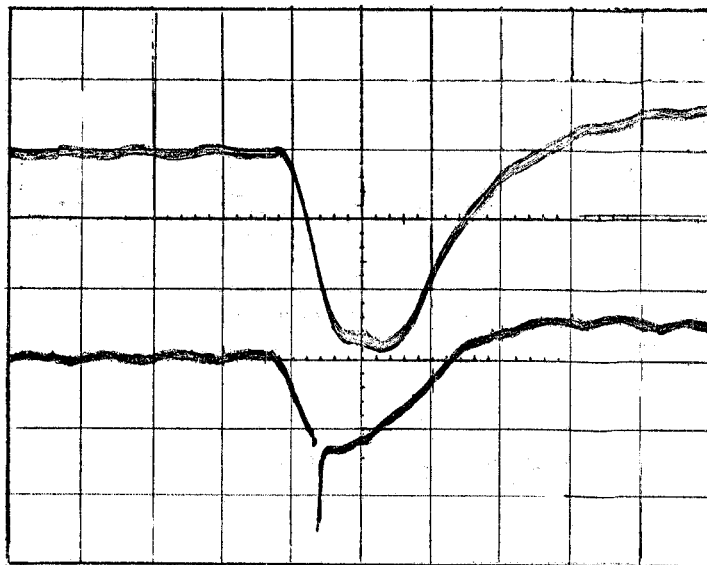FIG. A. 2 - Wiring diagram of the capacimeter.

FIG. A. 3 - Oscilloscope picture showing the expansion curves and the
beam arrival pulse.

tic field at every picture in order to overcome the lack of the current sta bilization of the magnet supply. This measurement was done by means of a Hall probe placed in the magnet near the chamber. The reading was done at every beam arrival by sending in the probe a chopped direct cur rent pulse (200 μs).

The value of the output voltage was recorded, by means of a digi tal voltmeter, directly on the bubble chamber film. Part of the digital voltmeter (a 10 MHz scaler) was also used for monitoring the incident photon flux so that a number proportional to the magnetic field intensity and, alternatively, to the incident photon flux was recorded on the film. The beam monitor consisted essentially in a 5 radiation lengths lead converter followed by a scintillation counter, and a fast counting chain.

An a-posteriori and a fast counting chain calibration of the counts recorded on the film was done by comparison with the e^+e^- pair number produced in the bubble chamber. The calibration was replated several ti mes during the runs. The detailed features of the monitoring apparatus as well as the calibration results are reported elsewhere.

24.

REFERENCES -

(1) - Cambridge Bubble Chamber Group: Phys. Rev. Letters 13, 639 (1964); 13, 640 (1964); Proc. Intern. Symp. on Electron and Photon Interactions at High Energies, Hamburg (1965), vol. II, p. 21; Phys. Rev. 146, 994 (1966); 155, 1468 (1967); 155, 1477 (1967); 156, 1426 (1967); 163, 1510 (1967).

(2) - Aachen, Berlin, Bonn, Hamburg, Heidelberg, München Collaboration: Proc. Intern. Symp. on Electron and Photon Interaction at High Energies, Hamburg (1965), vol. II, p. 36; Nuovo Cimento 41, 270 (1966); 48, 262 (1967); 49, 504 (1967); Phys. Letters 23, 707 (1966); Nuclear Phys. B1, 668 (1967).

(3) - P. Stichel, M. Scholz, Nuovo Cimento 34, 1388 (1964); M. P. Locher, W. Sandhas, Z. Physik 195, 461 (1966).

(4) - R. Del Fabbro, M. De Pretis, R. Jones, G. Marini, A. Odian, G. Stoppini, L. Tau, Phys. Rev. 139, B701 (1965).